ISSN: 0976-3104
SPECIAL ISSUE (SCMDSA)
Gopinath and Prabu

THE IIOAB JOURNAL

ARTICLE OPEN ACCESS

CLASSIFICATION OF THYROID ABNORMALITIES ON THERMAL IMAGE: A STUDY AND APPROACH

M. P. Gopinath* and S. Prabu

School of Computer Science and Engineering, VIT University Vellore, Tamil Nadu, INDIA

ABSTRACT

Thermal distribution in human body is a natural indicator of abnormalities. Thermal imaging is a non – invasive screening method for monitoring the distribution of body temperature. The objective of this paper is to compare different classification techniques which suites for classification of Thyroid Data set from UCI Machine Learning Repository. In the view of study we propose classification of Thyroid Abnormalities using thermal image. The proposed technique is based on the following computational methods; the median filter for preprocessing, Otsu's technique for segmentation, Gabor filter and Gray-Level Co-Occurrence Matrix is used to extract the feature from the selected Region of Interest and classifier to classify inputs into normal or abnormal using Decision tree. The experiment is carried out with 51 Thermal image which consist of 30 abnormal (hyper and hypo) and 21 normal from a real human neck. The classification accuracy was significantly good and finally possible future directions are suggested.

Received on: 09th-Sep-2015
Revised on: 27th-Sep-2015
Accepted on: 28th– April-2016
Published on: 16th –May-2016

KEY WORDS

Thermal imaging; Feature extraction; Feature selection; Segmentation; classification

***Corresponding author:** Email: mpgopinath@vit.ac.in **Tel:** +91-9840697916

INTRODUCTION

Medical Digital Infrared Thermal Imaging (DITI) is a new non – destructive adjunctive diagnostic technique that allows engineering projects to examine to visualize and measure the skin temperature by scanning the skin surface[1], scanning device converts the heat emitted by the skin and convert to signals that are captured as image. This color image maps the body temperature known as thermo gram. Skin tissue temperature is extracted by Penne's bio heat equation which is general heat diffusion equations [2]:

$$\rho C \frac{\partial T}{\partial t} = \nabla \left(k \nabla T \right) + W_b C_b \left(T_a - T \right) + q_m \qquad [1]$$

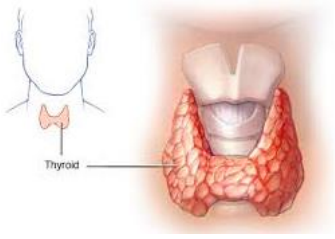

Fig 1a. Normal Thyroid Gland location

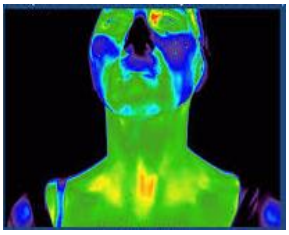

Fig 1b. Thermal image of Neck shows even distribution heat

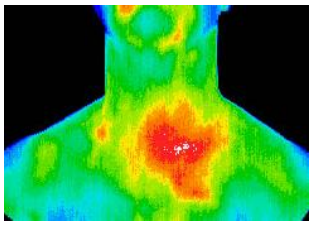

Fig 1c. Thermal Image of Neck shows uneven distribution of heat

THE IIOAB JOURNAL ISSN: 0976-3104

Thermal image system forms an image using infrared radiation and operates in wavelength as long as 14,000nm (14µm). The principal of temperature rises is the amount of radiation emitted by an object also increases. Every object has its own absorption and emission of thermal energy when any eccentricity happen it shows the stress of that object. Inflammation in human tissue shows the difference in distribution of heat around the body as any rapid changes happens automatically blood flow will increase in that particular place shows the abnormality of that part which can be identified by Penne's bio heat equation.

Thermal imaging or Thermography is the mapping of temperature distribution on the surface of the object or component. This technique is based on Infrared radiations. **Figure -1b** shows the normal distribution of heat ranges under control, **Figure -1c** shows the abnormal emission of heat in specified area which can be classified as thyroid abnormalities depends on various other factor Any object > 0 k emits electromagnetic radiations. At ambient temperatures and above are predominately within the infrared band of electromagnetic spectrum. Using appropriate detectors these radiations can be converted to suitable electrical signals and displayed on the monitor. Infrared cameras are manufactured predominately in two wavelength ranges 3-6 µm and 7-14 µm for medical application Sensitivity of FLIR camera vary with various versions of camera or models. Thermal sensitivity is smallest temperature difference that can be detected by the camera. Eg. For an infrared camera with uncooled micro bolometer detector the temperature sensitivity may be 0.01 ^{0}C @ 30 ^{0}C whereas for an infrared camera with semiconductor type of detector the temperature sensitivity may be 25mK @ 30 ^{0}C. Thermal image this captured from heat emitted from human body. Thyroid gland is responsible for all metabolic activity which increase blood flow and hormonal change which can be sensed by thermal camera. FLIR Thermal cameras with sensitivity of 0.01c with temperature range from -200c to +1200c are used for capturing thermal image [3].

Thyroid disorder is due to variation in TSH chemicals (hormones) that help the body to control metabolism. Thyroid hormone is normally produced in response to another hormone released by the pituitary gland. There are four main types of thyroid disease hyperthyroidism (too much thyroid hormone), hypothyroidism (too little thyroid hormone), benign (noncancerous). A thyroid disorders is an abnormal growth of cells within the thyroid gland or inside the throat, which can be cancerous (malign). It is defined as any intracranial tumor created by abnormal and uncontrolled cell division. Benign type of thyroid disorders can lead to Hyperthyroidism, Hypothyroidism, goiter, and thyroid nodules (benign/malignant). Detection of thyroid disorders in the earliest stage is the key for its successful treatment. The mean temperature with standard deviation of neck shows the thyroid abnormalities like hyperthyroid when temperature distribution of 36.63 ± 0.56 °C, hypothyroid when temperature distribution of 34.93 ± 0.32 °C, for normal 35.76 ± 0.49 °C [4,5]

The paper is organized as follows section 2presents various steps involved in thermal image diagnosis system with implementation of algorithm step by step specified in **Figure 2**, Section 3 presents different types of classification algorithm using UCI Thyroid data set repository, Section 4 Analysis the result of classification algorithm under specificity, sensitivity and accuracy, Section 5 presents the implementation and result discussion of proposed methods and shows the classified thyroid abnormalities in table6, Section 6 presents the conclusion and future work.

MEDICAL INFRARED THERMAL IMAGE DIAGNOSIS SYSTEM

Figure 2 shows the steps followed in proposed system. The development of thermal image diagnosis system helps in screening, prognosis and surgical procedures. Median filter is used for preprocessing Thermal image that taken by FLIR camera, enhancement using histogram equalization. Region of Interest (ROI) extracted manually Otsu Thresholding technique. Features were extracted and classified using Decision tree.

THE IIOAB JOURNAL
ISSN: 0976-3104

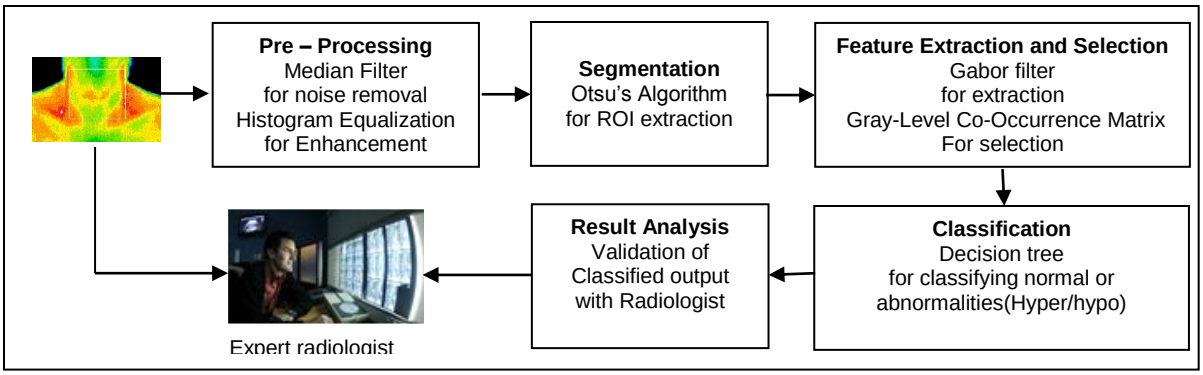

Fig: 2. Typical methodology of Thermal Image diagnosis system

Preprocessing

Filters is a method for modifying the image and remove noise from images which are classified as Linear and Non – Linear Filters. Linear filter will not preserve edges and losses fine minute details. Non – Linear filter preserve the information without any significant loss [6]. Median filters are one of the most popular nonlinear filters for removing salt and pepper noise through the image pixel by pixel, replacing the each value by the median value of center neighborhood shown in **Figure- 3**.

$$V(m,n) = median\left(y(m-k,n-l),(k,l)W\right) \qquad [2]$$

Where W chosen window

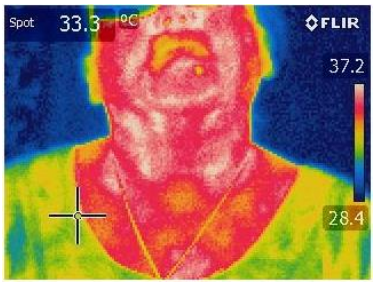

Fig 3a: Thermal image

Fig 3b: Preprocesed image

Image Enhancement

Image enhancement is used for sharpening, of image features such as edges or contrast to make an analysis. Histogram modeling is continuous process function[7]. Therefore the image intersection contains continuous intensity levels and the transformation function *f* which maps an input image *A(x,y)* onto output image *B(x,y)* is continuous within interval (0,1). The output probability densities of image enhancement is equal fraction of maximum number of intensity levels in the input image D_m. the transfer function necessary to achieve this result is simple. Result is shown in **Fig5**.

$$d\ (D_A)\ =\ D_M * P_A(D_A) \qquad [3]$$

Therefore

$$f(D_A) = DM\int_0^{DA} pA(U)du = DD_m * F_A(D_A) \qquad [4]$$

THE IIOAB JOURNAL
ISSN: 0976-3104

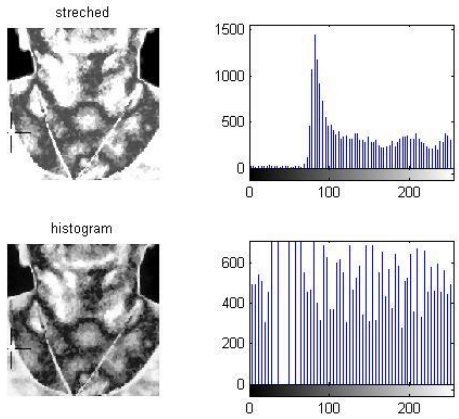

Fig :4a. Histogram Equalization (Streached)

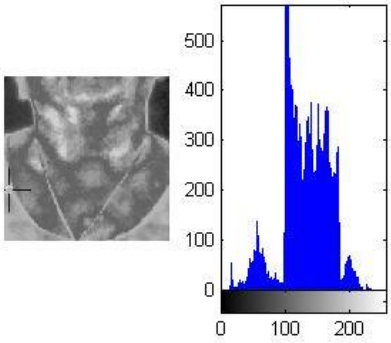

Fig: 4b. Histogram Equalization

Image Segmentation

Region of Interest is extracted manually from the region from binary image through Otsu Thresholding method[8] which is used to extract an object from its background by assigning an intensity value T through pixel by pixel is classified as an object point when ROI is segmented and shown in **Figure-7**.

Interclass variance is defined as

$$\sigma^2_{within}(T) = \omega B(T)\sigma^2_B(T)\sigma^2_0(T) \quad [5]$$

Where

$$\omega B(T) = \sum_{i=0}^{L-1} P(i) \quad [6]$$

(0,L-1] the range of intensity levels

$$\omega 0(T) = \sum_{i=0}^{L-1} P(i) \quad \omega 0(T) = \sum_{i=0}^{L-1} P(i) \quad [7]$$

$\sigma^2_B(T) = the\ varience\ of\ \ pixel\ in\ background\ below\ threshold$

$\sigma^2_0(T) = the\ varience\ of\ \ pixel\ in\ \ foreground\ above\ \ threshold$

$$\sigma^2_{Between}(T) = \sigma^2 - \sigma^2_{within}(T) = n_B(T)\left[\mu_B(T) - \mu\right]^2 + \left[\mu_0(T) - \mu\right]^2 \quad [8]$$

μ^2 $-is\ the\ combined\ varience$

$\mu - is\ the\ combined\ mean\ of\ the\ pixel\ Xi$

$$\sigma^2_{Between}(T) = n_B(T)n_0(T)\left[\mu_B(T) - \mu_0(T) - \mu\right]^2 \quad [9]$$

The standard deviation for any region with N pixels of intensity i = 1, 2, 3, ….N is given by

$$s = \sqrt{\sum_{i=1}^{N}(x_i - x)^2 / N}$$

Where x is the mean of x_i by substituting this we get

$$\sigma^2_{Between}(T) = n_B(T)n_0(T)\left[S_B(T) - S_0(T)\right]^2 \quad [10]$$

THE IIOAB JOURNAL ISSN: 0976-3104

S_B *is the standard deivation for background pixels*

S_0 *is the standard deivation for object pixels*

Using the threshold value T, the given input image *f(x, y)* is transformed to binary image *g(x, y)* as:

$$g(x,y) = \begin{cases} i\,if\ f(x,y) \geq T \\ 0\,otherwise \end{cases}$$

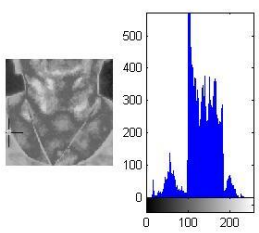

Fig: 5a. Input image for Segmantation **Fig: 5b. Segmented Image** **Fig: 5c.Thresholded Image**

Feature Extraction and Selection

This filter extract distinguishable texture features from the Gabor filtered image or global information image [9, 10]. It usually comprises of a complex exponential centered at a given frequency modified by a Gaussian envelop. This filter has real and imaginary parts because of the complex exponential. The 2D Gabor function provides the local spectral energy density, which particularly concentrates around the given position and frequency.

$$G(x, y, k_x, k_y) = \exp\left\{\frac{-(x-X)^2+(y-Y)^2}{2\sigma^2}\right\} e^{j(k_x^X + k_y^Y)} \qquad [11]$$

Where,
x, y - spatial coordinates
K_x, k_y - frequency coordinates
X, Y - spatial localizations of the Gaussian window.
It is self-similar and can be generated from wavelet by dilation and rotation. The pixel intensity of the global feature image is used to calculate feature vectors. The Gabor filters capture the spatial dependence with less ability and has low accuracy rate.

Gray-Level Co-Occurrence Matrix (GLCM) is a statistical method that includes the spatial relationship of pixels also known as gray-level spatial dependence matrix. The spatial relationship can be defined as the pixel of interest and the pixel to its direct right. The second order statistical texture features are extracted using GLCM. A GLCM is a matrix where the number of rows and columns are equal to the number of gray levels in the image. Based on the GLCM, parameters namely energy, contrast, entropy and correlation are computed. The texture feature extraction using GLCM involves following steps

- The R, G, B planes of images are separated.
- The GLCM matrices are calculated for each plane.

THE IIOAB JOURNAL ISSN: 0976-3104

Parameters of GLCM

Features	Formula
Energy	$\sum_i \sum_j P^2(i,j)$
Entropy	$\sum_i \sum_j P(i,j) \log P(i,j)$
Contrast	$\sum_i \sum_j (i-j)^2$
Homogeneity	$\sum_i \sum_j \frac{P(i,j)}{1+\lvert i-j \rvert}$

The statistical features, energy, entropy, correlation and contrast are computed for each GLCM matrix. The feature vector is calculated by using the means and variances of all parameters. GLCM is calculated from different combination of pixel brightness values occur in a pixel pair. It has high discrimination accuracy and requires less computational time.

CLASSIFICATION ALGORITHM

Decision Tree

A decision tree is a tree structure like graph, where each internal node indicates a test on an attribute [11]. Each branch represents an outcome of the test condition and each leaf node holds a class label. The decision tree classifier consist of two phases

- Growth phase or Build phase
- Pruning phase

The tree is constructed by repeatedly splitting the training set based on local optimal criteria. The second phase, handles the problem of over fitting the data in the decision tree. It generalizes the tree by removing the noise and outliers. Pruning phase increases the accuracy of the classification. It handles non-parametric data and does not require any design and training process. It provides hierarchical association between input variables to prediction class membership and offers a set of decision rules. These rules are easy to interpret and computational efficiency is high. The computational complexity occurs, when there exist undecided values and correlated outcomes.

THE IIOAB JOURNAL
ISSN: 0976-3104

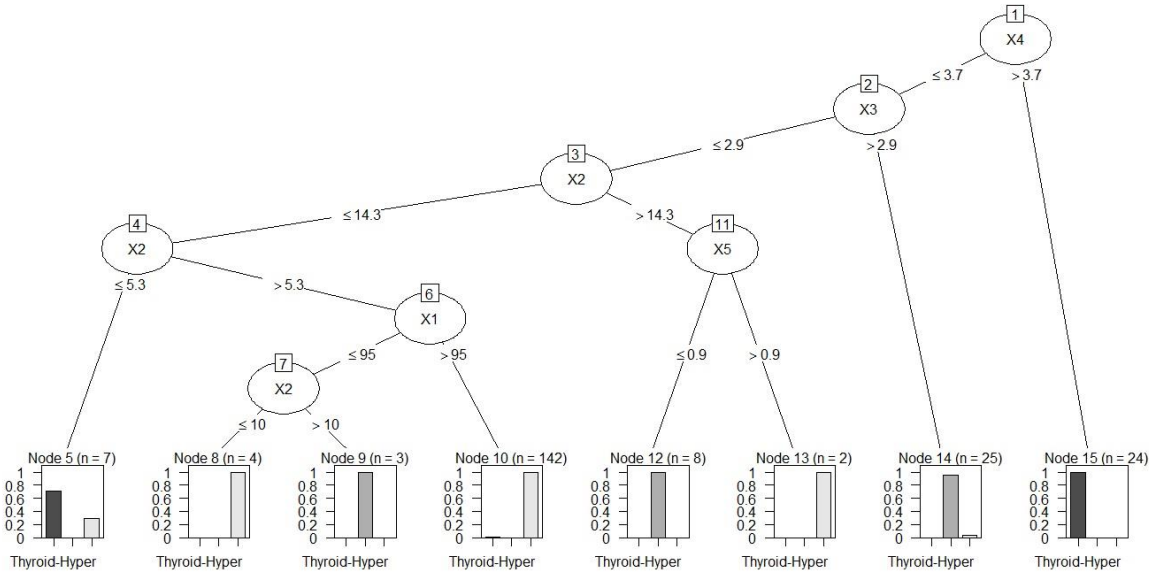

Fig: 6. Classification of data set using Decission tree

Naive Bayes

A Naive Bayes classifier is a family of probabilistic classifier works by applying Bayes' theorem [12]. It is simple method for generating classifiers that assign labels of finite set to vector of features that are selected will be treated as Independent features. For example thyroid gland is normal it produce even distribution of heat and have shape of butterfly. It considers each of these attribute as independent to the probability of classifying thyroid as normal, irrespective of possible correlation between features.

Conditional probability model to a given problem classified by vector $X = (x_1, ..., x_n)$ representing n features

$p(C_k \mid x_1, ..., x_n)$ k possible outcomes of class

$$p(C_k \mid X) = \frac{p(C_k)\, p(X \mid C_k)}{P(X)}$$

Using chain rule

$$p(C_k, x_1, \ldots, x_n) = p(C_k)\; p(x_1, \ldots, x_n \mid C_k) \qquad [12]$$

Under the independent assumption

$$p(C_k \mid x_1, \ldots, x_n) = \frac{1}{Z}\, p(C_k) \prod_{i=1}^{n} p(x_i \mid C_k)$$

Where $Z = p(x)$ the scaling factor depends on $x_1, \ldots, x_n$

THE IIOAB JOURNAL
ISSN: 0976-3104

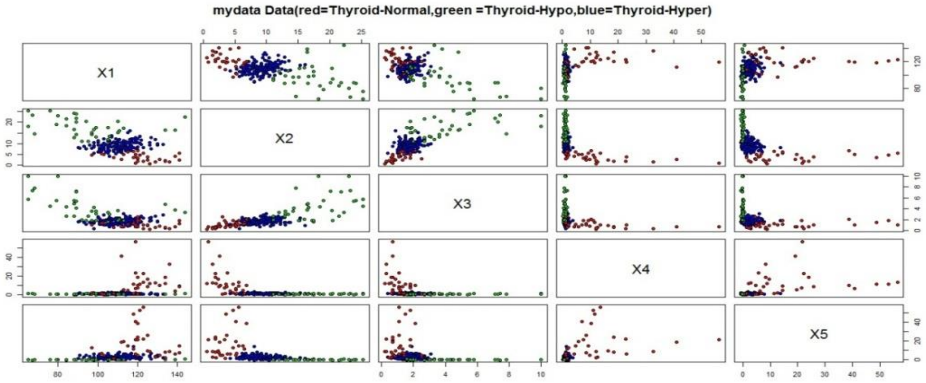

Fig: 7. Classification of data set using Naïve Bayes Classifier

Support Vector Machine (SVM)

SVM is a binary classifier and classifies two instance classes by identifying the maximum separation hyper plane. SVM in simpler form is termed as linear classifier and a non-linear SVM can be created by increasing the dimensionality of the feature space. A SVM constructs a hyper plane or set of hyper planes in a high or infinite dimensional space [13]. It uses a non-parametric with binary classifier approach and handles input data effectively and efficiently. The performance and accuracy of SVM depends on the hyper plane selection and kernel parameter. The result transparency in SVM is low and the structure of algorithm is difficult to understand. Bolster Vector Machine (SVM) models are a nearby cousin to established multilayer perceptron neural systems. Utilizing a portion capacity, SVM"s are an option preparing strategy for polynomial, spiral premise capacity and multi-layer perceptron classifiers in which the weights of the system are found by taking care of a quadratic solving so as to program issue with straight requirements, instead of a non-raised, unconstrained minimization issue as in standard neural system preparing. In the speech of SVM writing, an indicator variable is called a trait, and a changed ascribe that is utilized to characterize the hyper plane is known as a component. The errand of picking the most suitable representation is known as highlight determination. An arrangement of elements that portrays one case is known as a vector. So the objective of SVM displaying is to locate the ideal hyper plane that isolates groups of vector in a manner that cases with one class of the objective variable are on one side of the plane and cases with the other classification are on the other size of the plane. The vectors close to the hyper plane are the bolster vector.

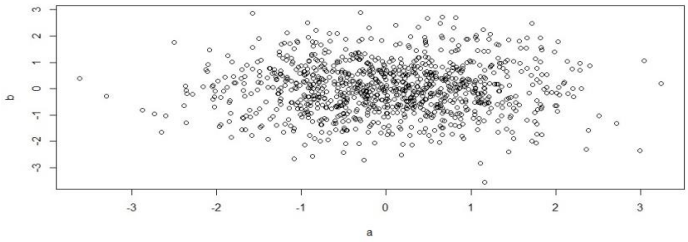

Fig :8. Classification of data set using SVM Classifier

Artificial Neural Network

An Artificial Neural Network (ANN), more often than not called neural network (NN), is a numerical model or computational model that is enlivened by the structure and/or useful parts of natural neural systems. A neural network comprises of an interconnected gathering of manufactured neurons, and it forms data utilizing a connectionist way to deal with calculation [14]. By and large an ANN is a versatile framework that progressions its structure taking into account outer or inward data that moves through the system amid the learning stage. Current neural systems are non-straight measurable information demonstrating apparatuses. Neural system models in manmade brainpower are typically alluded to as manufactured neural systems (ANNs); these are basically straightforward scientific models characterizing a capacity $f: X \rightarrow Y$ or a circulation over X or both X and Y, yet now and then models are likewise personally connected with a specific learning calculation or learning tenet. A

THE IIOAB JOURNAL
ISSN: 0976-3104

typical utilization of the expression ANN show truly implies the meaning of a class of such capacities. Simulated Neural Networks (ANN) has been produced as speculations of numerical models of organic sensory system.

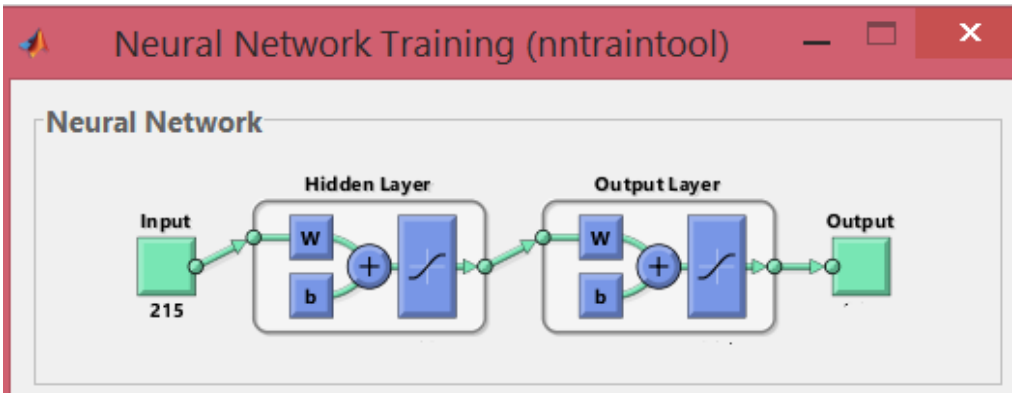

Fig: 9. Artificial Neural Network

$$f(x) = K\left(\sum_i w_i\, g_i(x)\right) \qquad [13]$$

K – *Activation function*

$f(x)$ –*Neural network function*

$g_i(x)$ – *Composition of other function*

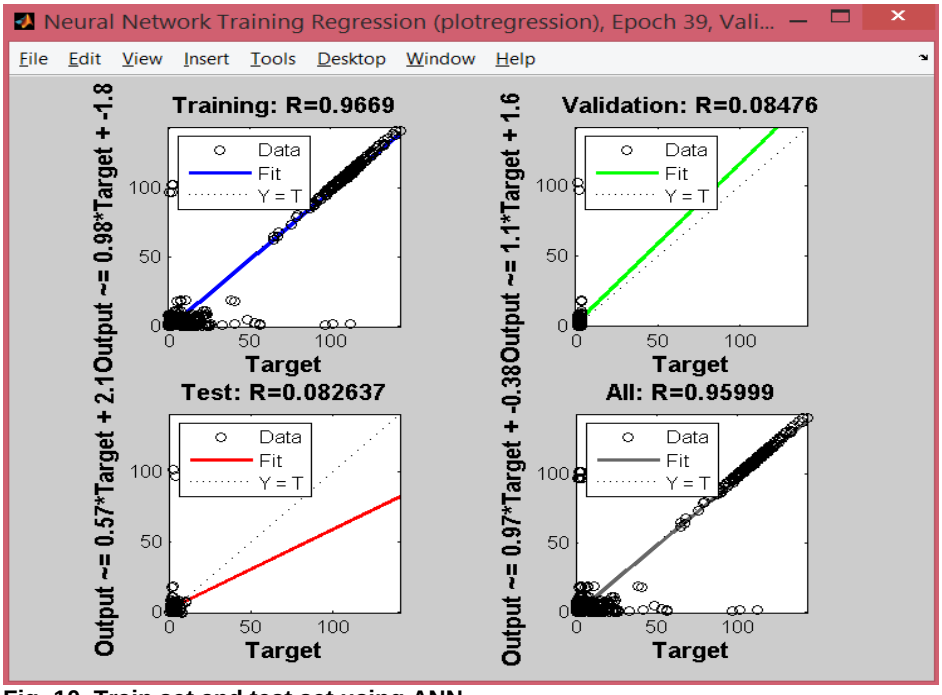

Fig: 10. Train set and test set using ANN

CLASSIFICATION ALGORITHM RESULTS AND DISCUSSION

Dataset: The data is been taken from online uci repository.*archive.ics.**uci**.edu/*

THE IIOAB JOURNAL ISSN: 0976-3104

Simulation result

Algorithm (Total Instances 215)	Correctly Classified Instance (% Values)	Incorrectly Classified Instance (%Values)	Time Taken In Secs	Kappa Statistic
Decision Tree	211(81.7757)	4(18.224)	0.23	0.9606
Naïve Bayes	152(71.0280)	62 (28.9703)	0.03	0.4321
Artificial Neural Network	170 (79.4392)	44 (20.5607)	16.67	0.5560
Support Vector Machine	173 (80.8411)	41 (19.1588)	0.67	0.5302

Training and error result:

Algorithm (Total Instances 214)	Mean Absolute Error	Root Mean Squared Error	Relative Absolute Error (%)	Root Relative Squared Error (%)
Decision Tree	0.2318	0.3772	50.5261	78.7789
Naïve Bayes	0.3005	0.4992	65.4846	104.2402
Artificial Neural Network	0.2177	0.4279	47.4360	89.3519
Support Vector Machine	0.2018	0.4492	43.9748	93.8086

Table 1: Classification Result

Confusion matrix:

Decision Tree

		Predicted		
		Normal	**Hypo**	**Hyper**
Actual	Normal	147	0	1
	Hypo	1	35	0
	Hyper	2	0	29
		.95	0.99	0.98
		Sensitivity	Specificity	Accuracy

Table 2: Decision Tree Confusion Matrix

Naïve Bayes

		Predicted		
		Normal	**Hypo**	**Hyper**
Actual	Normal	149	0	1
	Hypo	1	34	0
	Hyper	4	0	26
		.98	0.87	0.97
		Sensitivity	Specificity	Accuracy

Table 3: Naïve Bayes Confusion Matrix

Artificial Neural Network

		Predicted		
		Normal	**Hypo**	**Hyper**
Actual	Normal	145	0	0
	Hypo	0	35	0
	Hyper	1	0	29
		.98	0.87	0.79
		Sensitivity	Specificity	Accuracy

Table 4: Artificial Neural Network Confusion Matrix

THE IIOAB JOURNAL
ISSN: 0976-3104

Support Vector Machine

		Predicted		
		Normal	**Hypo**	**Hyper**
Actual	Normal	150	1	5
	Hypo	0	34	0
	Hyper	0	0	25
		.98	0.87	0.80
		Sensitivity	Specificity	Accuracy

Table 5: Support Vector Machine Confusion Matrix

Classification Result Discussion:

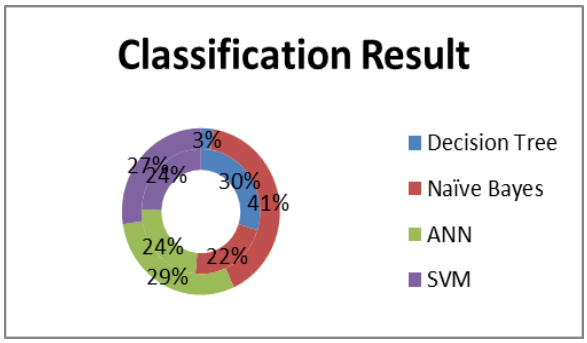

Fig 11: Classification result Graph

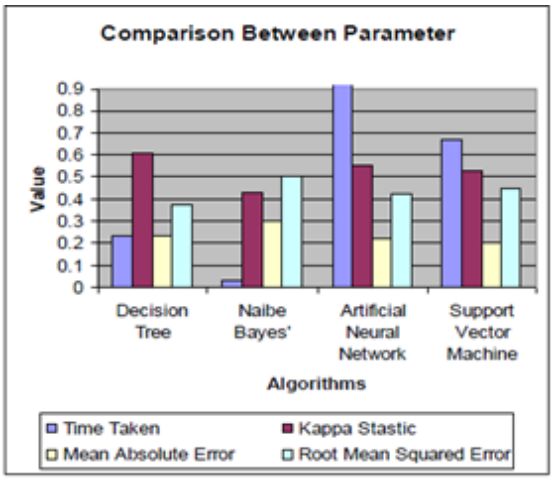

Fig 12: Comparison between parameter Graph

THE IIOAB JOURNAL
ISSN: 0976-3104

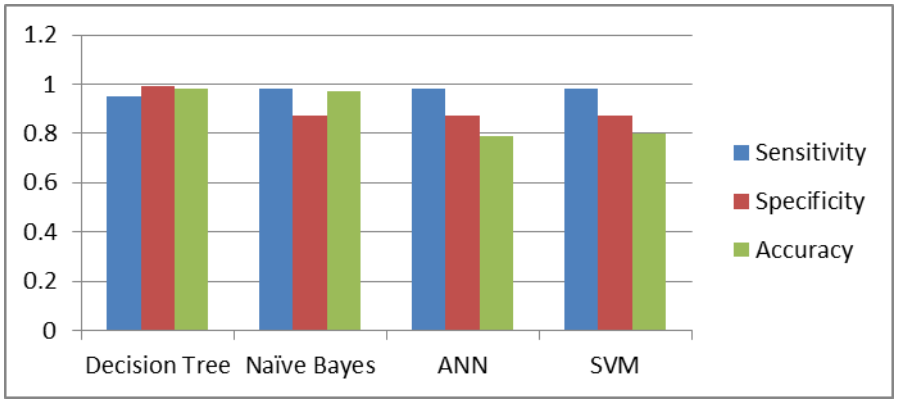

Fig 13: Confusion Matrix Graph

Classification Result Discussion

Decision tree classifier effectively grouped 214 occasions in 0.23 seconds. The erroneously arranged examples are 61 and Kappa measurement is 0.6132 for Decision Tree classifier. This examination recommends that Decision Tree classifier is the ideal calculation with maximum exactness for the charge card information. Despite the fact that, Naïve Bayes took 0.03 seconds to fabricate the model yet its precision is low. The dataset contain missing qualities. The test come about vigorously relies on upon the capacity to handle missing qualities by specific calculation. These outcomes demonstrate that among the machine learning calculations tried, the Decision Tree classifier can possibly fundamentally enhance customary characterization techniques in monetary part.

PROPOSED METHODOLOGY

Image acquisition and Data set

The algorithms where implemented based 51 real thermal image of neck consist of 21 normal and 30 abnormalities of which 14 hyperthyroidism and 16 hypothyroidism. The image captured by FLIR- E30 has temperature range of -20 to 250^{o} C with an accuracy of ±2% and thermal sensitivity of <0.10^{o}C produces thermal image of 160 x 120 resolutions. These images were collected from DITI India.

Preprocessing

Preprocessing is the first stage of medical image analysis used to reduce the noise and improve image resolution which improves the quality of image. First step of preprocessing is to convert color image to gray and remove noise from the image without affecting the edge, nonlinear filter removes the noise and preserve the edge. Median filter works by moving the window (pattern of neighbor pixels) through pixel by pixel over the image. Medial filter has special it is nonlinear for two sequence of X(m) and Y(m), Median(X(m) + Y(m)) not equal to median X(m) + median Y(m). 3.b shows the gray scale image after applying median filter. 4.a and 4.b shows the histogram equalize image .

Segmentation

We apply Otsu Thresholding to segment ROI in the Thermal Image manually. This method extract object from its background using intensity value T. **Figure- 5b** shows the segmented ROI and **Figure- 5c** shows the result of Thresholding using Otsu Algorithm. For analysis optimal threshold is taken to be 0.85 for all images. **Figure -14** shows sample thermal image before and after segmentation.

THE IIOAB JOURNAL
ISSN: 0976-3104

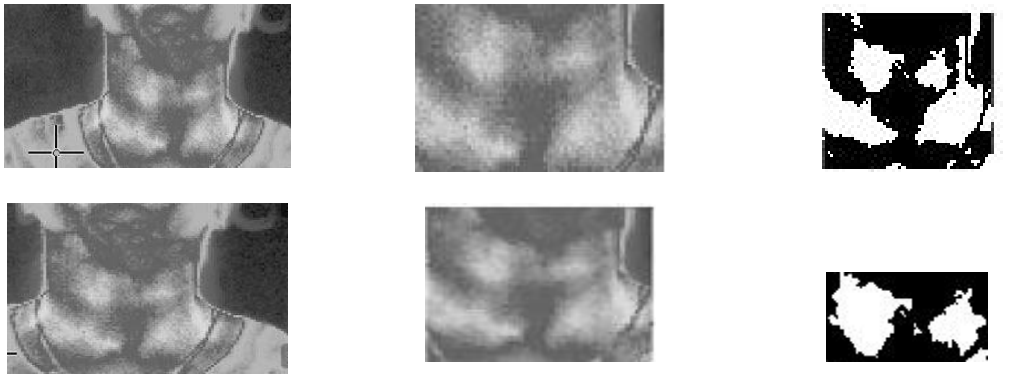

Before Segmentation ROI After Segmentation

Fig: 14. Sample Thyroid Thermal Image Before and after Segmentation using Otsu Algorithm

Feature Extraction and Feature Selection

Feature like area, mean, Variance and standard deviation are calculated and shown in **Table- 6**. For our analysis we have taken the area below 43 is categorized as normal all others abnormal, variance below 5.30 are normal and above is abnormal, standard deviation below 33 are normal all other abnormal.

Sl.No/ Image	Area	Standard Deviation	Variance	Temperature range	Identified	Expert Radiologist
1.IR_0403	33	18.66	4.32	36.15°C	Normal	Normal
2.IR_0419	4	38.81	6.23	36.50°C	Hyper	Abnormal
3.IR_0437	34	41.47	6.44	35.40°C	Hypo	Abnormal
4.IR_0467	19	27.24	5.22	36.24°C	Normal	Abnormal
5.IR_0509	4	38.96	6.17	37.20°C	Hyper	Abnormal
6.IR_0527	48	44.35	6.66	37.30°C	Hyper	Abnormal
7.IR_0563	41	37.45	6.12	38.10°C	Hyper	Abnormal
8.IR_0625	33	34.69	5.89	35.25°C	Hypo	Abnormal
9.IR_0927	48	24.70	4.97	36.10°C	Normal	Normal
10.IR_1013	45	25.00	5.00	35.90°C	Normal	Normal
11.IR_1019	13	16.97	4.12	35.24°C	Normal	Normal

Table: 6. Calculate values of parameter and classified result compared with expert radiologist

THE IIOAB JOURNAL
ISSN: 0976-3104

Classification

From the abnormal it has been classified as hyper and hypo using Decision tree classification algorithm

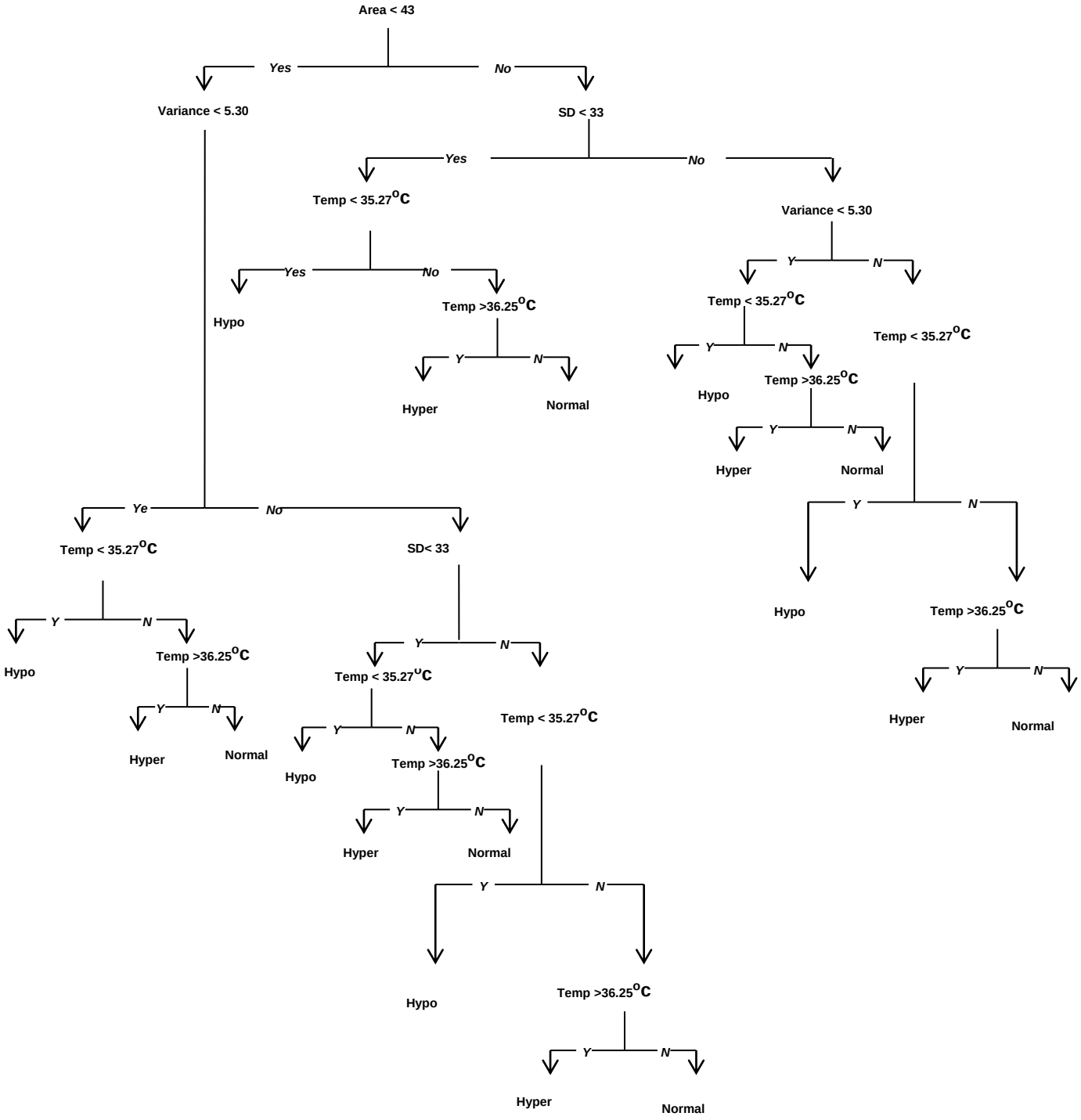

Fig: 15. Decision tree Classification for the Thyroid abnormalities

THE IIOAB JOURNAL
ISSN: 0976-3104

DISCUSSION

For the result analysis area below 43 is normal and above is abnormal, variance below 5.30 are normal and above are abnormal standard deviation below 33 are normal and above are abnormal using this parameter. For classifying abnormalities mean heat distribution value less than 35.27 are hypothyroidism, ranges from 35.27 – 36.25 are normal and greater than 36.25 are hyperthyroidism

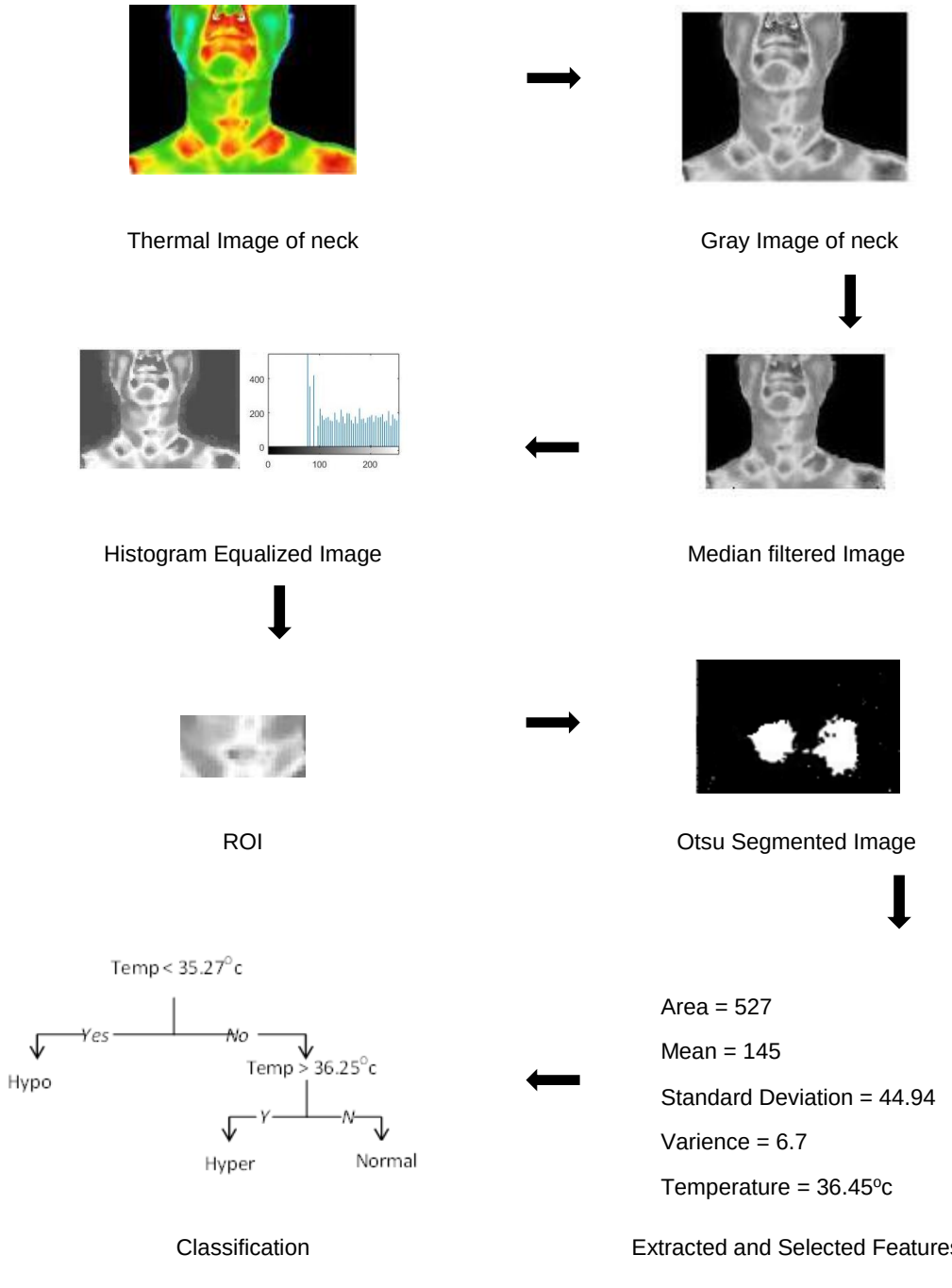

Fig 16. Proposed Mrthodology of Thyroid Thermal Image Classification

CONCLUSION

THE IIOAB JOURNAL
ISSN: 0976-3104

With the advancement in computational intelligence detection through thermography attracts more attention for medical analysis. Thermography is an easy non distractive technology for analyzing medical image by sensing heat emitted by human body. Thermography can be used for detecting and classifying thyroid abnormalities by simple mapping with body temperature. Thermography is one of major research subjects in medical imaging and diagnosis system. With the survey we proposed a methodology classification of thermal image. The proposed technique first apply median filter and histogram equalization for noise removal and image enhancement on converted gray scale image, then by using Otsu segmentation ROI is extracted, then employs Gabor filter and GLCM to extract features from Thermal image and by using the selected features decision tree algorithm classify as hyperthyroid, hypothyroid or normal. Result discussion on proposed method shows the robustness of proposed techniques. According to the experimental result proposed method propose classification accuracy of 95% with 96% sensitivity rate and 92% specificity rate. The challenges remain to provide generalized approach that works in all cases regardless of data base size and quality. Thermal Image Diagnosis system remains an open problem: (1) Acquisition of large database from different centers with various image qualities. (2)We have noticed segmentation plays vital role in ROI which is considered for our feature work. (3)Inclusion of machine learning techniques with hybrid model will increase the classification accuracy.

FINANCIAL DISCLOSURE

No financial support was received to carry out this project.

ACKNOWLEDGEMENT

This work is part of Ph. D Research work. It is not supported by any agency
.

CONFLICT OF INTERESTS

Authors declare no conflict of interest.

REFERENCES

[1] Lahiri, B. B., Bagavathiappan, S., Jayakumar, T., & Philip, J. (2012). Medical applications of infrared thermography: a review. *Infrared Physics & Technology*, *55*(4), 221-235.

[2] Viglianti, B. L., Dewhirst, M. W., Abraham, J. P., Gorman, J. M., & Sparrow, E. M. (2014). Rationalization of thermal injury quantification methods: application to skin burns. *Burns*, *40*(5), 896-902.

[3] Calin, M. A., Mologhianu, G., Savastru, R., Calin, M. R., & Brailescu, C. M. (2015). A review of the effectiveness of thermal infrared imaging in the diagnosis and monitoring of knee diseases. *Infrared Physics & Technology*, *69*, 19-25.

[4] Rossato, M., Burei, M., & Vettor, R. (2015). Neck thermography in the differentiation between diffuse toxic goiter during methimazole treatment and normal thyroid. *Endocrine*, *48*(3), 1016-1017.

[5] Mahajan, P., & Madhe, S. (2014, August). Hypo and hyperthyroid disorder detection from thermal images using Bayesian Classifier. In *Advances in Communication and Computing Technologies (ICACACT), 2014 International Conference on* (pp. 1-4). IEEE.

[6] Nur, R., & Frize, M. (2013, March). Image processing of infrared thermal images for the detection of necrotizing enterocolitis. In *SPIE Medical Imaging* (pp. 86692M-86692M). International Society for Optics and Photonics.

[7] Tyagi, M. S., Amhia, M. H., & Tyagi, M. S. (2013). Comparative Study of Image Enhancement and Analysis of Thermal Images Using Image Processing and Wavelet Techniques. *International Journal of Computational Engineering Research*, *3*(4), 32-38.

[8] Purushotham, S., & Tripathy, B. (2014). A comparative study of RIFCM with other related algorithms from their suitability in analysis of satellite images using other supporting techniques. *Kybernetes*, *43*(1), 53-81.

[9] Etehadtavakol, M., Ng, E. Y. K., Chandran, V., & Rabbani, H. (2013). Separable and non-separable discrete wavelet transform based texture features and image classification of breast thermograms. *Infrared Physics & Technology*, *61*, 274-286.

[10] Bhattacharya, S., & Deepa, N. (2013). Non-Contact Dry Eye Syndrome Diagnosis using Thermal Imaging and GLCM Feature. In *Proc. of Int. Conf. on Advances in Computer Science and Application* (pp. 759-763).

[11] Mestha, L. K., & Venkataramani, K. (2016). *U.S. Patent No. 20,160,135,729*. Washington, DC: U.S. Patent and Trademark Office.

[12] Acharya, U. R., Tan, J. H., Vidya, S., Yeo, S., Too, C. L., Lim, W. J. E., ... & Tong, L. (2014).

THE IIOAB JOURNAL
ISSN: 0976-3104

Diagnosis of response and non-response to dry eye treatment using infrared thermography images. *Infrared Physics & Technology*, *67*, 497-503.

[13] Acharya, U. R., Ng, E. Y. K., Tan, J. H., & Sree, S. V. (2012). Thermography based breast cancer detection using texture features and support vector machine. *Journal of medical systems*, *36*(3), 1503-1510.

[14] Haddadnia, J., Hashemian, M., & Hassanpour, K. (2013). Diagnosis of Breast Cancer using a Combination of Genetic Algorithm and Artificial Neural Network in Medical Infrared Thermal Imaging. *Iranian Journal of Medical Physics*, *9*(4), 265-274.

[15] Mohanaiah, P., Sathyanarayana, P., & GuruKumar, L. (2013). Image texture feature extraction using GLCM approach. *International Journal of Scientific and Research Publications*, *3*(5), 1.

[16] Mitra, J., Martí, R., Oliver, A., Lladó, X., Ghose, S., Vilanova, J. C., & Meriaudeau, F. (2012). Prostate multimodality image registration based on B-splines and quadrature local energy. *International journal of computer assisted radiology and surgery*, *7*(3), 445-454.

[17] Skala, K., Lipić, T., Sović, I., Gjenero, L., & Grubišić, I. (2011). 4D thermal imaging system for medical applications. *Periodicum biologorum*, *113*(4), 407-416.

[18] Pašagić, V., Mužević, M., & Kelenc, D. (2008). Infrared thermography in marine applications. *Brodogradnja*, *59*(2), 123-130.

[19] Hildebrandt, C., Raschner, C., & Ammer, K. (2010). An overview of recent application of medical infrared thermography in sports medicine in Austria. *Sensors*, *10*(5), 4700-4715.

[20] Chang, C. Y., Chung, P. C., Hong, Y. C., & Tseng, C. H. (2011). A neural network for thyroid segmentation and volume estimation in CT images. *Computational Intelligence Magazine, IEEE*, *6*(4), 43-55.

[21] Forsberg, F., Machado, P., Segal, S., Okamura, Y., Guenette, G., Rapp, C., & Lyshchik, A. (2014, September). Microvascular blood flow in the thyroid: Preliminary results with a novel imaging technique. In *Ultrasonics Symposium (IUS), 2014 IEEE International* (pp. 2237-2240). IEEE.

[22] Luo, S., Kim, E. H., Dighe, M., & Kim, Y. (2009, September). Screening of thyroid nodules by ultrasound elastography using diastolic strain variation. In *Engineering in Medicine and Biology Society, 2009. EMBC 2009. Annual International Conference of the IEEE* (pp. 4420-4423). IEEE.

[23] Lavarello, R. J., Ridgway, B., Sarwate, S., & Oelze, M. L. (2013, April). Imaging of follicular variant papillary thyroid carcinoma in a rodent model using spectral-based quantitative ultrasound techniques. In *Biomedical Imaging (ISBI), 2013 IEEE 10th International Symposium on* (pp. 732-735). IEEE.

[24] Savelonas, M. A., Iakovidis, D. K., Legakis, I., & Maroulis, D. (2009). Active contours guided by echogenicity and texture for delineation of thyroid nodules in ultrasound images. *Information Technology in Biomedicine, IEEE Transactions on*, *13*(4), 519-527.

[25] El-Dahshan, E. S. A., Mohsen, H. M., Revett, K., & Salem, A. B. M. (2014). Computer-aided diagnosis of human brain tumor through MRI: A survey and a new algorithm. *Expert systems with Applications*, *41*(11), 5526-5545.

ABOUT AUTHORS

Prof. M.P.Gopinath is working as Assistant Professor (Senior) in School of Computing Science and Engineering, VIT University, Vellore. His research area includes Image processing, data mining. He has published 4 journal papers in his research filed. He is life member of CSI and IEEE. He is also part of various school activity committees.

Dr. S. Prabu is working as Associate professor in the school of computing sciences and engineering, VIT University, at Vellore, India. He is the principal Investigator of Funded project from SAC-ISRO. He is life member of CSI and IEEE. He has published many technical papers in various international journals, conferences, and Springer book chapters. His research interest includes Image processing, Remote Sensing, Cloud Computing.